PHYSICAL REVIEW C **78**, 064613 (2008)

Microscopic optical potential for α-nucleus elastic scattering in a Dirac-Brueckner-Hartree-Fock approach

Wei Zou (邹巍),[1,2] Yuan Tian (田源),[1] and Zhong-Yu Ma (马中玉)[1,3]
[1]*China Institute of Atomic Energy, P.O. Box 275(18), Beijing 102413, People's Republic of China*
[2]*Department of Physics, Jilin University, Jilin 130023, People's Republic of China*
[3]*Center of Theoretical Nuclear Physics, National Laboratory of Heavy Collision, Lanzhou 730000, People's Republic of China*
(Received 10 July 2008; published 29 December 2008)

The microscopic optical model potential (OMP) of α-nucleus elastic scattering based on a double-folding model (DFM) is studied. The nucleon OMPs in nuclear matter as well as the nucleon-nucleon (NN) effective interaction are calculated in the framework of the Dirac-Brueckner-Hartree-Fock (DBHF) approach, in which the density and energy dependence is parametrized by polynomial expansions. The microscopic OMP of nucleus-nucleus scattering is obtained by doubly folding the complex NN effective interaction with respect to the densities of both projectile and target nuclei. An improved local-density approximation is adopted to take account of the finite-range correction. Renormalization factors on the real and imaginary OMP are introduced to obtain the best fit to the experimental data. A systematic analysis of ^{4}He elastic scattering off ^{12}C, ^{16}O, ^{28}Si, and ^{40}Ca is performed. The calculated cross sections over a wide range of incident energies and scattering angles are in good agreement with the experimental data, which confirms the applicability of this model. Moreover, for the same projectile and target, the renormalization factors are found to be almost constant at various incident energies.

DOI: 10.1103/PhysRevC.78.064613 PACS number(s): 25.55.Ci, 21.30.Fe, 24.10.Ht, 24.10.Jv

I. INTRODUCTION

The study of the microscopic optical model potential (OMP) of nucleus-nucleus elastic scattering is one of the fundamental subjects in nuclear physics. It has attracted much attention for a long time and recent renewed interest owing to the development of the physics of unstable nuclei. The microscopic OMP is important not only for understanding the relevant reaction dynamics involved but also for developing a practical tool in the study of colliding systems for which the elastic scattering measurement is absent or difficult, such as in the case of neutron-rich or proton-rich β-unstable nuclei. The double-folding model (DFM) is one of the simplest and most practical tools for constructing the OMP between complex nuclei. In the DFM, the nucleon-nucleon (NN) effective interaction in the nuclear medium is doubly folded with nucleon density distributions of both projectile and target nuclei. One of the most successful effective NN interactions is the so-called M3Y G-matrix interaction [1] and its density- and energy-dependent versions, such as CDM3Y6 [2,3]. The DFM with the CDM3Y6 interaction, however, provides us only with the real part of the NN OMP and an imaginary potential must be added by hand [4,5]. Normally, the imaginary potential is assumed to have some suitable functional forms [6,7], such as a Woods-Saxon form or its derivative, and the potential parameters included are determined phenomenologically so as to reproduce the experimental elastic-scattering data. In addition, the so-called frozen approximation for the density in the NN effective interaction, which is assumed in this approach, may overestimate the overlap of two colliding nuclei. Another successful example employed by the DFM is the so-called JLM folding model [8–10]. In this model a complex Brueckner Hartree-Fock (BHF) G-matrix interaction is adopted, so both real and imaginary parts of the OMP can be obtained at the same time. Unfortunately, the nucleon effective interactions were parametrized a long time ago, when the BHF approach without a three-body force could not reproduce the nuclear matter saturation properties. The relativistic microscopic optical potential (RMOP) of nucleon scattering off nucleus has been discussed for many years [11–13]. Recently, the Dirac-Brueckner-Hartree-Fock (DBHF) approach has been of great success in describing the isospin-dependent RMOP of nucleon-nucleus scattering [14]. By considering the target as just a scatterer the nucleus-nucleus scattering was obtained by folding the isospin-dependent nucleon-nucleus OMP with respect to the density of the projectile [15]. The ^{4}He scattering off ^{12}C and ^{6}He + ^{12}C elastic scattering differential cross sections were reproduced. In this paper we parametrize the density and energy dependence of the nucleon OMP in nuclear matter as well as the NN effective interaction with polynomial expansions. The OMPs of the nucleus-nucleus scattering are obtained by a double-folding method with the NN effective interaction. They are applied to a systematic analysis of ^{4}He elastic scattering off ^{12}C, ^{16}O, ^{28}Si, and ^{40}Ca in this work. In the present calculations the geometric average of the individual densities in the nucleus-nucleus scattering is assumed. The effect of the density overlap will be further investigated in sequential works later.

The outline of this paper is as follows. The theoretical framework of the double-folding potential of nucleus-nucleus scattering is described briefly in Sec. II. The nucleon OMPs in nuclear matter are parametrized by polynomial expansions. In Sec. III, the cross sections of α scattering off ^{12}C, ^{16}O, ^{28}Si, and ^{40}Ca at various incident energies are analyzed systematically. Finally, we give a summary and conclusions in Sec. IV.

II. THEORETICAL FRAMEWORK

A. Parametrizations of the nucleon OMP in nuclear matter

It is well known that the nucleon self-energy in the nuclear medium is equivalent to the nucleon OMP [16]. The energy- and density-dependent nucleon self-energy in nuclear matter can be calculated in the DBHF approach [12,14]. A detail description of the nucleon self-energy obtained in the DBHF approach is presented in Refs. [12,14,15]. For the sake of completeness of this paper, we report briefly the method to obtain the nucleon self-energy in the DBHF. The DBHF G can be decomposed into the bare NN interaction V and a correlation term ΔG, where $G = V + \Delta G$ [17]. The bare NN interaction is depicted by meson exchanges and the Bonn B NN interaction is adopted here. The correlation term is parametrized by four vertices: scalar, vector, isoscalar, and isovector. Because of the characteristics of the short-range correlation, they can be described by infinite masses and finite ratios of strengths to the corresponding masses [17]. The nucleon self-energy in nuclear matter is calculated with V and ΔG in the relativistic Hartree-Fock approach. The general form of the self-energy of a nucleon in nuclear matter can be written as [14]

$$\Sigma(|\mathbf{k}|, k_F, \beta) = \Sigma_s(|\mathbf{k}|, k_F, \beta) - \gamma_0\Sigma_0(|\mathbf{k}|, k_F, \beta) + \gamma\cdot\mathbf{k}\Sigma_v(|\mathbf{k}|, k_F, \beta), \quad (1)$$

where Σ_s, Σ_0, and Σ_v are the scalar potential and time, space components of vector potentials, respectively. They are functions of the nucleon momentum, density, and asymmetry parameter $\beta = (\rho_n - \rho_p)/\rho$, where ρ_n, ρ_p, and ρ are neutron, proton, and matter densities, respectively. The imaginary part of the nucleon self-energy can be obtained by the G-matrix polarization diagram. An effective nucleon interaction was introduced to avoid difficulties caused by π mesons and simplify the calculation [14]. Four scalar and vector mesons with density-dependent coupling constants were adopted to reproduce the saturation curves and nucleon self-energy at various densities and asymmetric parameters calculated with the DBHF G matrix. The isovector mesons allow the potentials for neutrons and protons to be distinguished.

The Dirac equation of a nucleon in the nuclear medium with scalar and vector potential has the form

$$[\alpha\cdot\mathbf{k} + \gamma_0(M + U_s) + U_0]\psi = E\psi, \quad (2)$$

where

$$U_s = \frac{\Sigma_s - M\Sigma_v}{1+\Sigma_v}, \quad U_0 = \frac{-\Sigma_0 + E\Sigma_v}{1+\Sigma_v}. \quad (3)$$

In these expressions, M is the mass of nucleons, U_s and U_0 are Lorentz scalar and vector potentials, respectively, $E = \varepsilon + M$, and ε is the kinetic energy of the nucleon in the free space. Its momentum in the nuclear medium can be calculated by solving the following equation:

$$E = \sqrt{k^2(1+\Sigma_v)^2 + (M+\Sigma_s)} - \Sigma_0. \quad (4)$$

The Schrödinger-equivalent equation for the upper component of the Dirac spinor can be obtained by eliminating the lower component of the Dirac spinor in a standard way,

$$\left[\frac{k^2}{2E} + U_{\rm eff}\right]\varphi = \frac{E^2 - M^2}{2E}\varphi, \quad (5)$$

where

$$U_{\rm eff} = \frac{M}{E}U_s + U_0 + \frac{1}{2E}[(U_s)^2 - (U_0 + V_C)^2], \quad (6)$$

where V_C is the Coulomb potential for protons. $U_{\rm eff}$ is the Schrödinger-equivalent potential, which is known as the nucleon OMP in nuclear matter in the nonrelativistic approach and is complex with both real and imaginary parts.

The nucleon OMP in the nuclear medium depends on the density and the nucleon energy. To simplify the calculation we parametrize the density and energy dependence of the nucleon OMP in polynomial expansions. This procedure changes the numerical results into an analytical form and is convenient for application in the DFM calculations. The scattering energy is chosen as $\varepsilon \leqslant 120$ MeV and the density as $\rho < 0.22$ fm^{-3}. In the DFM we do not distinguish proton and neutron effective interactions; therefore only the isoscalar part of the OMP is adopted in this work.

The parametric forms of the real and imaginary parts of the nucleon OMP in nuclear matter can be expressed as

$$\mathrm{Re}U_{\rm eff}(\rho,\varepsilon) = \sum_{i=1}^{3}\sum_{j=1}^{3} a_{ij}\varepsilon^{j-1}\rho^i \quad (7)$$

and

$$\mathrm{Im}U_{\rm eff}(\rho,\varepsilon) = \sum_{i=1}^{4}\sum_{j=1}^{4} b_{ij}\varepsilon^{j-1}\rho^i, \quad (8)$$

where the coefficients a_{ij} and b_{ij} are gathered in Tables I and II, respectively. The real and imaginary parts of the OMP at energies $\varepsilon = 10, 30, 60, 90$, and 120 MeV are shown as functions of the density ρ in Figs. 1 and 2, respectively. The solid points are obtained in the DBHF [Eq. (6)] and the curves are calculated with the parametrizations in Eqs. (7) and (8). It is clearly shown that the nucleon OMP in nuclear matter calculated in the DBHF approach can be fairly well reproduced by the parametrizations.

To compare with the JLM model [8], the nucleon OMPs in the JLM model are also plotted in Figs. 1 and 2 with dashed curves. The nucleon OMPs in the JLM model were calculated in the framework of the BHF approximation with Reid's hard-core NN interaction. It is well known that the BHF calculations with Reid's hard-core NN interaction produce binding energies that are too small at the nuclear matter saturation density [18,19]. Therefore the real parts of the nucleon OMP obtained in the JLM model are relatively weaker than those obtained in our DBHF calculations with the Bonn B NN interaction, especially at low densities. The parametrizations in the JLM model were constructed within the nuclear saturation density $k_F = 1.4$ fm^{-1}. The extension to

TABLE I. Values of the coefficients a_{ij} in Eq. (7).

a_{ij}	1	2	3
1	-0.797×10^3	0.222×10^1	-0.825×10^{-3}
2	0.366×10^4	-0.438×10^1	-0.696×10^{-2}
3	-0.515×10^4	0.584×10^1	0.221×10^{-1}

TABLE II. Values of the coefficients b_{ij} in Eq. (8).

b_{ij}	1	2	3	4
1	-0.503×10^2	-0.426×10^1	0.270×10^{-1}	-0.328×10^{-4}
2	0.203×10^3	0.636×10^2	-0.601×10^0	0.163×10^{-2}
3	0.829×10^3	-0.416×10^3	0.408×10^1	-0.122×10^{-1}
4	-0.348×10^4	0.958×10^3	-0.100×10^2	0.327×10^{-1}

high densities may give unphysical results, which are shown in Fig. 1. To reproduce the nuclear saturation properties in the BHF approximation inclusion of a three-body force or relativistic effects is necessary, both of which play roles mainly at the density above the saturation density. The difference in the imaginary parts of the OMPs between the JLM model and our approach is quite large, as shown in Fig. 2. Unfortunately, the imaginary part of the BHF G matrix is not well constrained and depends on the bare NN interaction adopted in the BHF calculations. It was found that the imaginary part of the G matrix is sensitive to the π-meson exchange [14]. The imaginary parts of the OMP in the JLM model are much larger at low energies and tend to a surface-like shape at high energies, they become very weak at the saturation density as the energy increases. It is clearly seen in Fig. 2 that the extension of the imaginary OMP with the JLM parametrizations to high densities approaches zero and even becomes positive, which is of course unphysical. The imaginary part of the nucleon OMP in our model is calculated by the effective nucleon interaction $G_{\rm eff}$, which consists of four effective meson exchanges that reproduce the real part of the nucleon self-energies and properties of symmetric and asymmetric nuclear matter [14]. The imaginary parts of the nucleon OMP in our model increase monotonically as the energy increases.

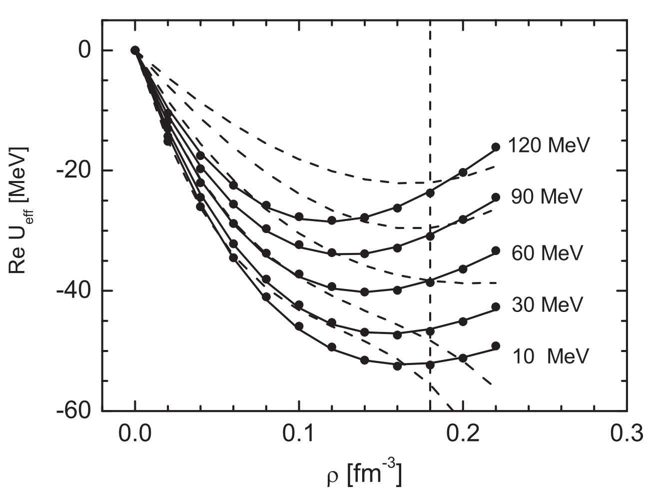

FIG. 1. The density dependence of the real part of the nucleon OMPs in nuclear matter at the energies $\varepsilon = 10, 30, 60, 90,$ and 120 MeV. Points are calculated in the DBHF approach [14]. The solid and dashed curves show the results calculated with the parametrizations in the present DBHF approach and JLM model [8], respectively. The vertical dashed curves shows the validity domain of the JLM model.

B. Double-folding potential of nucleus-nucleus elastic scattering

The NN effective interaction can be connected with the nucleon OMP in the nuclear medium by $V_{\rm eff} = U_{\rm eff}/\rho$ in the Thomas-Fermi approximation [20]. The OMP of the nucleus-nucleus scattering is then obtained by doubly folding the NN effective interaction in the nuclear medium with nucleon density distributions of both projectile and target nuclei:

$$V_{\rm DFM}(\mathbf{R}) = \int \rho_1(\mathbf{r}_1)\rho_2(\mathbf{r}_2)V_{\rm eff}(\mathbf{s}, \rho, \varepsilon)d\mathbf{r}_1 d\mathbf{r}_2, \tag{9}$$

where ρ_1 and ρ_2 are nucleon densities in the projectile and target nuclei, respectively, $\mathbf{s} = \mathbf{R} + \mathbf{r}_1 - \mathbf{r}_2$ is the relative vector between the interacting nucleon pair, $\mathbf{R}$ is the separation distance between two centers of colliding nuclei, and $\mathbf{r}_1$ and $\mathbf{r}_2$ are the coordinates of the nucleon in the center-of-mass frame of the projectile and target, respectively.

By taking account of the finite-range correlation an improved local density approximation (ILDA) with Gaussian form is introduced, which should yield good agreement between the theoretical and the empirical values of the volume integrals and rms radii of phenomenological OMP [8]. The finite-range form factor of the effective interaction is taken as

$$V_{\rm eff}^{\rm ILDA}(\mathbf{s}, \rho, \varepsilon) = g_R(\mathbf{s}){\rm Re}V_{\rm eff} + i g_I(\mathbf{s})\,{\rm Im}V_{\rm eff}, \tag{10}$$

where

$$g(\mathbf{s}) = (t\sqrt{\pi})^{-3}\exp(-\mathbf{s}^2/t^2), \tag{11}$$

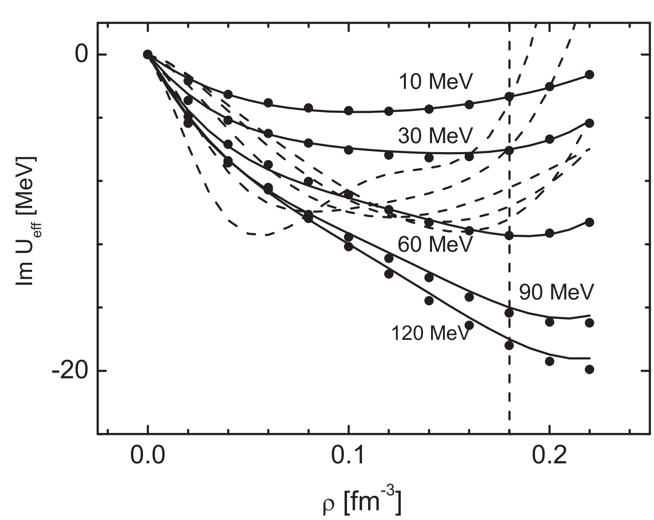

FIG. 2. Same as Fig. 1 for the imaginary part of the nucleon OMPs in nuclear matter.

and t is the range of the Gaussian form. In our calculations we choose $t_R = 1.1$ fm for the real potential and $t_I = 1.8$ fm for the imaginary one. One notices that the NN effective interaction $V_{\rm eff}^{\rm ILDA}$ depends on the scattering density ρ through Eqs. (7) and (8). It is not clear how to choose the density of the two interacting nucleons, which are populated in the projectile and target nuclei, respectively. Two approximations were usually adopted in the literature [5,9]: the so-called frozen density approximation (FDA), $\rho(\mathbf{s}) = \rho_1(\mathbf{r_1} + \mathbf{s}/2) + \rho_2(\mathbf{r_2} - \mathbf{s}/2)$, and the geometric average of the individual density [9],

$$\rho(\mathbf{s}) = \sqrt{\rho_1(\mathbf{r}_1 + \mathbf{s}/2)\rho_2(\mathbf{r}_2 - \mathbf{s}/2)}. \tag{12}$$

In both cases the density is evaluated at the midposition of the interacting nucleons. There is no physical justification for determining which approach is more appropriate, although it has been studied from several aspects [21,22]. It is observed that the elastic scattering of α particles and some tightly bound light nuclei has shown the pattern of rainbow scattering at medium energies. The observed rainbow patterns were shown to be linked directly to the density overlap of the two nuclei penetrating each other in the elastic channel [21]. The nucleus-nucleus interaction potentials studied in the time-dependent Hartree-Fock theory favor the FDA [22]. Actually the overlap density in heavy nucleus scattering is rather complicated, being also dependent on the properties of the projectile and target. We shall study this important issue later on. At the moment we adopt the geometric average of the individual density but simply take another type of prescription [9] in this paper,

$$\rho = \sqrt{\rho_1(\mathbf{r}_1)\rho_2(\mathbf{r}_2)}, \tag{13}$$

where the local density is evaluated at each position of two interacting nucleons. This choice also enables us to greatly reduce the computational time for numerical integrations.

III. RESULTS

Now we apply this scheme to systematically analyze α scattering off ^{12}C, ^{16}O, ^{28}Si, and ^{40}Ca nuclei. The OMP of the nucleus-nucleus scattering is calculated with the DFM. In this model, the density distribution of ^{4}He is simply calculated with the harmonic oscillator wave function,

$$\rho_\alpha = \frac{4}{\pi^{3/2} b_\alpha^3} \exp\left(-\frac{r^2}{b_\alpha^2}\right), \tag{14}$$

where $b_\alpha = 1.1932$ fm. This has an rms radius of 1.461 fm, which is close to the experimental value of 1.47 ± 0.02 fm. The density distributions of the targets, except for light nuclei ^{12}C and ^{16}O, are taken from Negele's empirical formulas [23],

$$\rho(r) = \frac{\rho_0}{1 + \exp[(r - r_0)/a]}, \tag{15}$$

where $\rho_0 = 3A/4\pi r_0^3(1 + \pi^2 a^2/r_0^2)$, $r_0 = (0.978 + 0.0206A^{1/3})A^{1/3}$ fm, and $a = 0.54$ fm, and A is the atomic number of the target. For the density distribution of ^{12}C, one takes $r_0 = 2.1545$ fm and $a = 0.425$ fm [3]. The density is normalized to the atomic number of ^{12}C, then ρ_0 is determined as 0.207 fm^{-3}. A Gaussian-type distribution is chosen for ^{16}O [24]:

$$\begin{aligned} \rho(r) &= \rho_0[1 + \alpha r^2/a^2]\exp(-r^2/a^2), \\ \rho_0 &= A \Big/ \left[4\pi a^3 \sqrt{\pi}\left(\frac{1}{4} + \frac{3}{8}\alpha\right)\right], \end{aligned} \tag{16}$$

where $\alpha = 2.0$ fm and $a = 1.76$ fm.

In recent years many accurate experimental data of α scattering by various stable nuclei at a wide range of incident energies below 240 MeV have become available. To reproduce the experimental data, we introduce renormalization factors N_R and N_I in the real and imaginary parts of the double-folding potentials, respectively. Accordingly, the OMP of the nucleus-nucleus elastic scattering can be redefined as

$$V_{\rm opt} = N_R {\rm Re}\, V_{\rm DFM} + i N_I\, {\rm Im}\, V_{\rm DFM}. \tag{17}$$

The values of N_R and N_I are adjusted in each case to attain an optimum fit to the experimental data of the elastic scattering cross sections. In this paper, we apply the χ^2 analysis,

$$\chi^2 = \sum_{i=1}^{N} \left(\frac{\sigma_i^{\rm cal} - \sigma_i^{\rm exp}}{\sigma_i^{\rm exp}}\right)^2, \tag{18}$$

where $\sigma_i^{\rm cal}$ and $\sigma_i^{\rm exp}$ are calculated and experimental cross sections, respectively. We compile an automatic potential search code to find the renormalization factors when χ^2 reaches a minimum.

First we analyze the reactions of ^{4}He elastic scattering off ^{12}C and ^{16}O, which are "refractive" targets and have attracted much attention. The cross sections, plotted in units of the Rutherford cross section, for ^{4}He scattering off ^{12}C at $E_{\rm Lab} =$ 104, 120, 145, 166, and 172.5 MeV are shown in Fig. 3. Correspondingly, the values of the renormalization factors, volume integrals, and rms radii of the real and imaginary parts of the RMOP are listed in Table III. One can see that the cross sections calculated with the nucleon effective interaction in Eqs. (7) and (8) based on the DBHF reproduce the experimental data quite well. At the same time, the renormalization factors are found to be almost constant ($N_{\rm R} \approx 0.63$–0.67 and $N_{\rm I} \approx 1.5$–1.8), showing a weak dependence on the energy in this energy region. More accurately, elastic scattering cross sections of ^{4}He off ^{12}C at $E_{\rm Lab} = 172.5$ MeV are plotted on a linear scale in Fig. 4. The scattering cross sections of ^{4}He + ^{16}O at $E_{\rm Lab} = 48.7$, 54.1, 69.5, 80.7, 104 MeV are shown in Figs. 5 and 6. Obviously, the available experimental data exhibit quite a strong refractive structure. It is shown in Figs. 5 and 6 that our OMP could well describe the feature of elastic scattering angular distributions at various incident energies. It is inspiring that the characteristic oscillatory patterns at $E_{\rm Lab} = 48.7$, 54.1, and 69.5 MeV, which cover a wide angular range, are fairly well reproduced, especially at the middle and backward angles. They have typical rainbow features, which are sensitive to the OMP over a wide radial domain. The renormalization factors $N_R \approx 0.7$–0.75 and $N_I \approx 1.7$–1.8 are required to reproduce the experimental data.

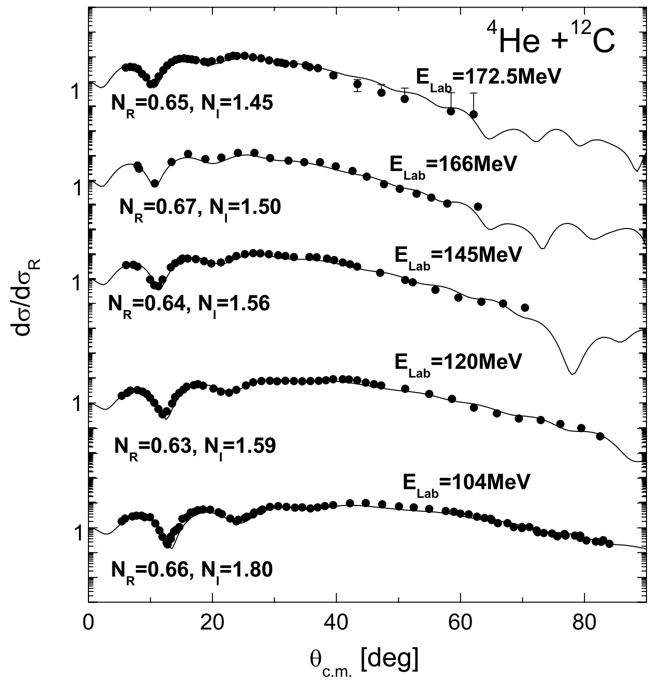

FIG. 3. ^{4}He elastic scattering off ^{12}C at the incident energies $E_{\text{Lab}} = 104$, 120, 145, 166, and 172.5 MeV. Solid curves show the results calculated with the OMP in this work. The renormalization factors N_R and N_I are listed in the figure. Points denote the experimental data taken from Refs. [25–27].

To further study the OMP, we also examine the reactions of ^{4}He elastic scattering off ^{28}Si at $E_{\text{Lab}} = 104$, 166, and 240 MeV and ^{40}Ca at $E_{\text{Lab}} = 40.05$, 47, 53.9, 80, 104, and 141.7 MeV. The calculated results are shown in Figs. 7 and 8 together with the available experimental data. Good agreement with the experimental data is also observed. For ^{4}He scattering off ^{40}Ca, the experimental nuclear rainbow phenomena are well reproduced over a wide range of scattering angle. The values of N_R and N_I for each target listed in Table III are found to be almost constant with respect to different incident energies. These results reconfirm the applicability of the NN effective interaction obtained based on the DBHF. The volume integral per nucleon pair and rms radii of the OMP for all the elastic scattering reactions are also listed in Table III.

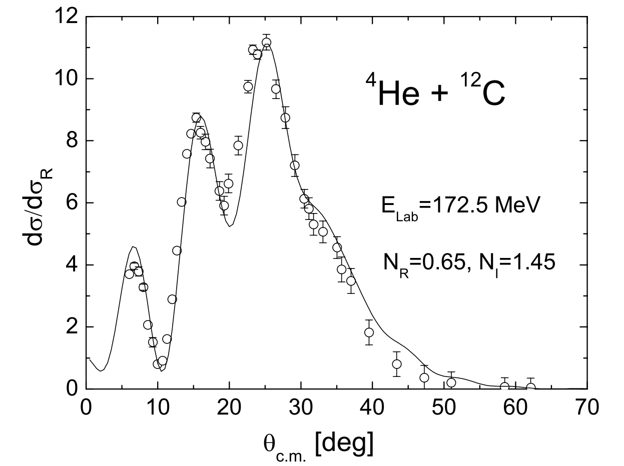

FIG. 4. ^{4}He elastic scattering off ^{12}C at the incident energy $E_{\text{Lab}} = 172.5$ MeV. The notation is the same as in Fig. 3.

TABLE III. Values of normalization factors N_R and N_I of the folding optical potentials for α scattering off ^{12}C, ^{16}O, ^{28}Si, and ^{40}Ca at various energies. Their volume integrals and rms radii are also listed.

Target	E_{Lab} (MeV)	N_R	N_I	J_R (MeV fm^3)	J_I	$\sqrt{\langle r^2\rangle_R}$ (fm)	$\sqrt{\langle r^2\rangle_I}$ (fm)
^{12}C	104	0.66	1.80	289	102	3.212	3.752
	120	0.63	1.59	272	98	3.219	3.761
	145	0.64	1.56	269	108	3.221	3.756
	166	0.67	1.50	276	113	3.223	3.748
	172.5	0.65	1.45	266	111	3.225	3.739
^{16}O	48.7	0.76	1.60	363	67	3.407	3.982
	54.1	0.75	1.68	356	74	3.407	3.988
	69.5	0.75	1.95	351	96	3.408	3.982
	80.7	0.73	1.83	338	97	3.407	3.979
	104	0.68	1.83	308	111	3.409	3.980
^{28}Si	104	0.58	1.74	260	106	3.873	4.437
	166	0.66	1.50	279	121	3.906	4.415
	240	0.64	1.25	250	126	3.916	4.383
^{40}Ca	40.05	0.71	1.45	329	54	4.157	4.673
	47	0.73	1.68	336	67	4.157	4.677
	53.9	0.72	1.90	329	80	4.158	4.679
	80	0.63	1.81	281	92	4.163	4.665
	104	0.63	1.68	274	99	4.164	4.669
	141.7	0.62	1.50	260	106	4.170	4.648

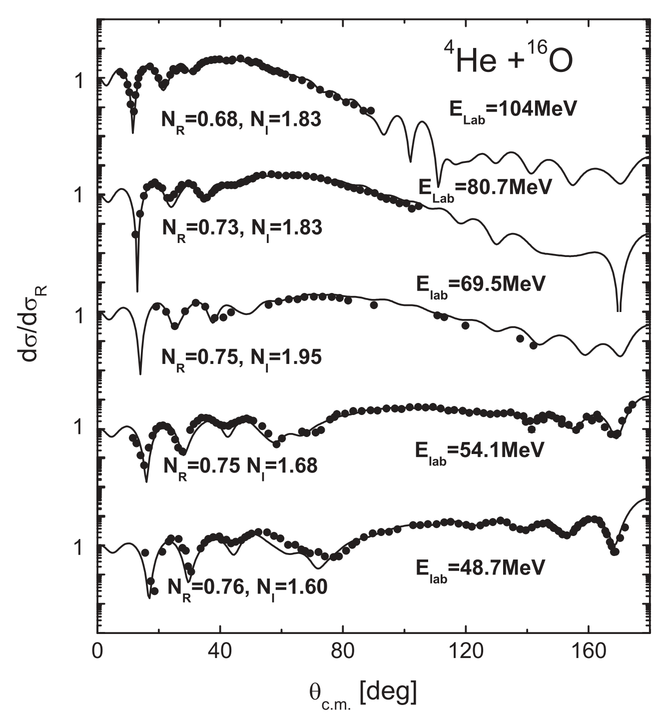

FIG. 5. Same as Fig. 3, except for ^{4}He elastic scattering off ^{16}O at the incident energies $E_{\text{Lab}} = 48.7$, 54.1, 69.5, 80.7, and 104 MeV. The experimental data are taken from Refs. [5,25,28].

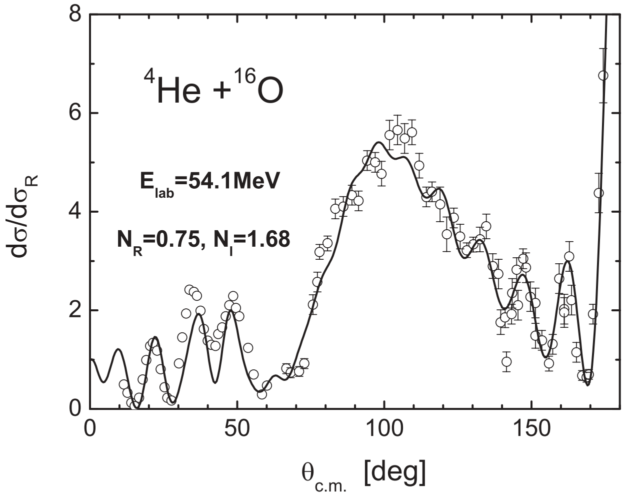

FIG. 6. ^{4}He elastic scattering off ^{16}O at the incident energy $E_{\rm Lab} = 54.1$ MeV. The notation is the same as in Fig. 3.

IV. SUMMARY

In this paper we parametrize the nucleon effective interaction in the nuclear medium based on the DBHF approach. The microscopic OMPs for α-nucleus elastic scattering are obtained by the DFM. To test its applicability, the elastic data of ^{4}He scattering on ^{12}C, ^{16}O, ^{28}Si, and ^{40}Ca targets at various incident energies $E_{\rm Lab}$ ranging from 40.05 to 240 MeV have been analyzed. All the experimental cross sections up to the backward angles are well reproduced by the double-folding potentials. We found that the renormalization factors of the real and imaginary parts of the OMP could be regarded as constants for the same projectile and target and weakly depend on the incident energies. These results may suggest that the double-folding potential with the nucleon effective interaction based on the DBHF approach has the predicting power of the complex optical potential for nucleus-nucleus scattering. For the same projectile and target, the renormalization factors obtained from one reaction could serve in other reactions. In this paper, we only test α-nucleus elastic scattering, so a further test of our model will be required. In the present investigation we adopt the geometric averaged density as the scattering density, which may underestimate the density effects. Therefore the renormalization factors for the real part are relatively small ($N_R \sim 0.7$). The overlap density may also depend on the structures of the two colliding nuclei. The density effects could be further investigated with the nuclear effective interactions applicable in a large density range obtained in this work. The imaginary part of the nucleon effective interaction derived from the lowest order contribution of the Dirac G matrix does not involve all the complex dynamic processes in heavy-ion scattering. Therefore, it is also desirable to include these dynamic processes in the imaginary part of the OMP.

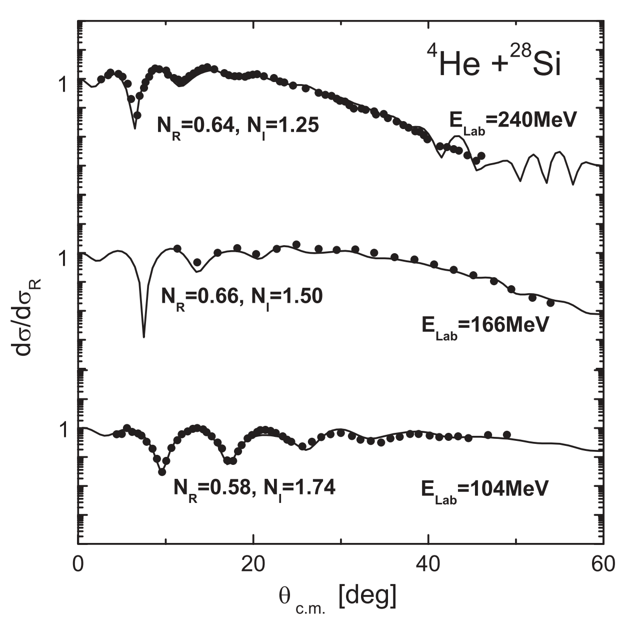

FIG. 7. ^{4}He elastic scattering off ^{28}Si at the incident energies $E_{\rm Lab} = 104$, 166, and 240 MeV. The notation is the same as in Fig. 3. The experimental data are taken from Refs. [25,27,29].

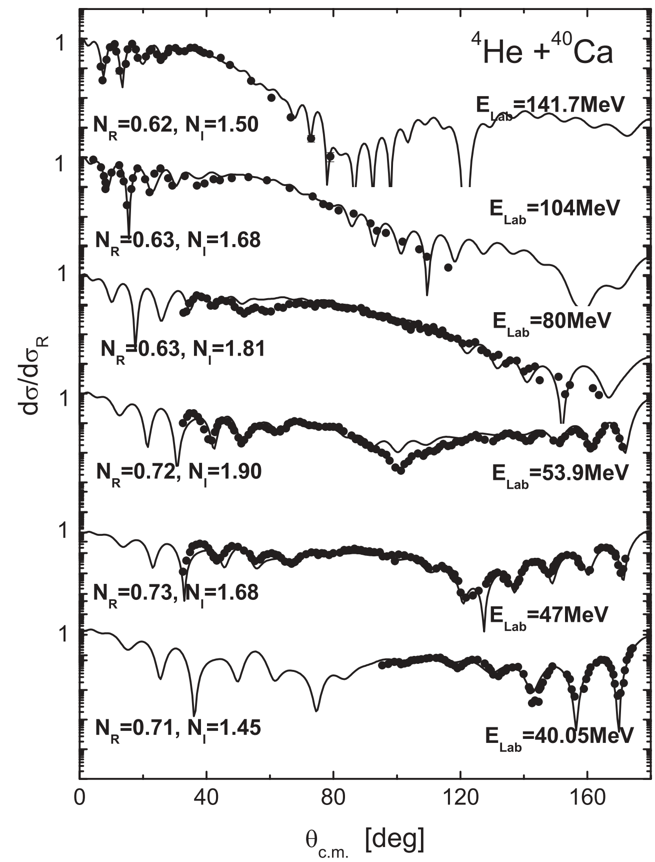

FIG. 8. ^{4}He elastic scattering off ^{40}Ca at the incident energies $E_{\rm Lab} = 40.05$, 47, 53.9, 80, 104, and 141.7 MeV. The notation is the same as in Fig. 3. The experimental data are taken from Refs. [25,30].

ACKNOWLEDGMENTS

This work is supported by the National Natural Science Foundation of China under Grant Nos. 10875150, 10775183, and 10535010 and by the Major State Basic Research Development Program in China under Contract No. 2007CB815000.

[1] G. Bertsch *et al*., Nucl. Phys. **A284**, 399 (1977).
[2] D. T. Khoa, G. R. Satchler, and W. von Oertzen, Phys. Rev. C **56**, 954 (1997).
[3] V. Lapoux *et al*., Phys. Rev. C **66**, 034608 (2002).
[4] G. R. Satchler and W. G. Love, Phys. Rep. **55**, 183 (1979).
[5] D. T. Khoa, Phys. Rev. C **63**, 034007 (2001).
[6] L. C. Chamon, D. Pereira, M. S. Hussein, M. A. Candido Ribeiro, and D. Galetti, Phys. Rev. Lett. **79**, 5218 (1997).
[7] M. A. G. Alvarez *et al*., Nucl. Phys. **A723**, 93 (2003).
[8] J. P. Jeukenne, A. Lejeune, and C. Mahaux, Phys. Rev. C **15**, 10 (1977); **16**, 80 (1977).
[9] F. Carstoiu and M. Lassau, Nucl. Phys. **A597**, 269 (1996).
[10] T. Furumoto and Y. Sakuragi, Phys. Rev. C **74**, 034606 (2006).
[11] Z. Ma, P. Zhu, Y. Gu, and Y. Zhuo, Nucl. Phys. **A490**, 619 (1988).
[12] Z.-Y. Ma and B.-Q. Chen, J. Phys. G **18**, 1543 (1992).
[13] B.-Q. Chen and A. D. Mackellar, Phys. Rev. C **52**, 878 (1995).
[14] J. Rong, Z. Y. Ma, and N. Van. Giai, Phys. Rev. C **73**, 014614 (2006).
[15] Y. Q. Ma, W. Zou, and Z. Y. Ma, J. Phys. G: Nucl. Part. Phys. **35**, 065108 (2008).
[16] J. S. Bell and E. J. Squires, Phys. Rev. Lett. **3**, 96 (1959).
[17] E. Schiller and H. Müther, Eur. Phys. J. A **11**, 15 (2001).
[18] B. D. Day, Comments Nucl. Part. Phys. **11**, 115 (1983).
[19] R. Machleidt, Adv. Nucl. Phys. **19**, 189 (1989).
[20] H. A. Bethe, Phys. Rev. **167**, 879 (1968).
[21] D. T. Khoa, W. von Oertzen, H. G. Bohlen, and S. Ohkubo, J. Phys. G: Nucl. Part. Phys. **34**, R111 (2007).
[22] K. Washiyama and D. Lacroix, Phys. Rev. C **78**, 024610 (2008).
[23] J. W. Negele, Phys. Rev. C **1**, 1260 (1970).
[24] H. F. Ehrenberg *et al*., Phys. Rev. **113**, 666 (1959).
[25] G. Hauser, R. Lohken, H. Rebel, G. Schatz, G. W. Schweimer, and J. Specht, Nucl. Phys. **A128**, 81 (1969).
[26] S. Wiktor, C. Mayer-Boricke, A. Kiss, M. Rogge, P. Turek, and H. Dabrowski, Acta Phys. Pol. B **12**, 491 (1981).
[27] I. Brissaud, M. K. Brussel, M. Sowinski, and B. Tatischeff, Phys. Lett. **B30**, 324 (1969).
[28] H. Abele, H. J. Hauser, A. Körber, W. Leitner, R. Neu, H. Plappert, T. Rohwer, G. Staudt, M. Strasser, S. Welte, M. Walz, P. D. Eversheim, and F. Hinterberger, Z. Phys. A **326**, 373 (1987).
[29] D. H. Youngblood, Y. W. Lui, and H. L. Clark, Phys. Rev. C **65**, 034302 (2002).
[30] H. P. Gubler, U. Kiebele, H. O. Meyer, G. R. Plattner, and I. Sick, Phys. Lett. **B74**, 202 (1978); Nucl. Phys. **A351**, 29 (1981).